Buffering the oxygen activity of uranium dioxide fuels using niobium and molybdenum as redox additives

Philippe Garcia, Erwin Douguet-Bronnec, Franck Fournet-Fayard, Florian Le Hello, Xavière Iltis, Nicolas Tarisien, Jacques Fouletier, Marlu Cesar Steil

Journal of Nuclear Materials
Volume 607, March 2025, 155647
https://doi.org/10.1016/j.jnucmat.2025.155647

Buffering the oxygen activity of uranium dioxide fuels using niobium and molybdenum as redox additives

Philippe Garcia[a], Erwin Douguet–Bronnec[a], Franck Fournet–Fayard[b], Florian Le Hello[a], Xavière Iltis[a], Nicolas Tarisien[a], Jacques Fouletier[b], Marlu Cesar Steil[b]

[a]*CEA, DES, IRESNE, DEC, Cadarache F–13108 Saint-Paul-Lez-Durance, France*
[b]*Univ. Grenoble Alpes, Univ. Savoie Mont Blanc, CNRS, Grenoble INP, LEPMI, F–38000, Grenoble, France*

Abstract

We demonstrate that it is possible to control the oxygen activity of a uranium oxide fuel by incorporating additives during the manufacturing process that have a strong redox activity. To this end, we have studied the macroscopic electrochemical properties of three polycrystalline uranium dioxide samples, the first containing both molybdenum and molybdenum dioxide, the second containing niobium dioxide and the last containing no additives other than impurities. During experiments, samples were subjected to reducing and subsequently oxidizing atmospheres with respect to the oxygen partial pressure at which the oxidized and reduced forms of the additives are in equilibrium. *In situ* monitoring of the electrochemical response of the samples reveals that the presence of redox couples involving either niobium or molybdenum significantly modifies the oxygen activity of a uranium dioxide solid. Scanning Electron Microscopy (SEM), Electron Back-Scatter Diffraction (EBSD) and Energy Dispersive X-ray analysis (EDX) prior to and following the high temperature measurements, confirm the *in situ* data: the final microstructure purports to show that the electrochemical activity is controlled by the Mo/MoO_2 and the NbO_2/Nb_2O_5 couples for the molybdenum and niobium containing samples respectively.

Keywords: uranium dioxide, non–stoichiometry, Nernst equation, chemical potential of oxygen, redox buffering, niobium oxides, molybdenum
PACS: 82.45.Xy, 82.33.Pt, 66.30.Ny

Email addresses: philippe.garcia@cea.fr (Philippe Garcia), erwin.douguet-bronnec@cea.fr (Erwin Douguet–Bronnec), franck.fournet-fayard@grenoble-inp.fr (Franck Fournet–Fayard), jacques.fouletier@lepmi.grenoble-inp.fr (Jacques Fouletier), marlu-cesar.steil@lepmi.grenoble-inp.fr (Marlu Cesar Steil)

1. Introduction

Many past studies have sought to use additives to enhance oxide fuel performance of Pressurized Water Reactors (PWRs) [1], in order to make them safer, extend their operating burnup or possibly alleviate constraints upon fuel assembly manoeuvrability. Studies relating to large grained materials [2], originally thought of to mitigate the effect of fission gas release, is one of the best examples although these studies have been met with varying degrees of success [3]. It is also a recurring proposition that in-reactor fuel chemistry may be key to understanding and hence eliminating the risk of zircaloy cladding failure due to stress corrosion cracking (SCC) during a pellet-cladding interaction (PCI) event [4]. Indeed, in a uranium dioxide fuel containing no additives, the oxygen activity of the solid slowly changes over time as oxygen is released by fission events. The local oxygen activity will depend upon many factors such as temperature, temperature gradient, the valence and mobility of fission products etc. The resulting oxygen activity is difficult to predict as it depends upon equilibrium and non-equilibrium thermodynamic and kinetic properties, that are in the main poorly known. The idea has therefore arisen that by adding a redox couple that could act as a buffer, the oxygen activity of a uranium dioxide fuel could to some extent be controlled or kept within a range that reduces the risk of PCI failure [5]; the strategy then being to maintain the putative corrosive agents such as iodine or tellurium, in physical forms that render them essentially innocuous in relation to SCC. Niobium has been investigated to this effect [6] but molybdenum [7] is also of interest. Indeed, although the conditions which the Mo/MoO_2 equilibrium is liable to impose upon the fuel are thought to be unfavorable in regard to iodine induced SCC [5], this redox couple is of interest because it is expected to be activated "naturally" in-pile as a result of molybdenum being a relatively abundant fission product: the oxygen potential of PWR oxide fuels is thought to increase as burnup proceeds but there is understandably a dearth of data in this respect. According to Matzke [8], the oxygen potential of a UO_2 fuel taken from the central part of the pellet should increase at 750°C from *circa* -450 kJ/mol to -390 kJ/mol at roughly 80 GWd/tU. This latter value is indeed close to the equilibrium oxygen potential of the Mo/MoO_2 couple at that temperature (-401 kJ/mol[9]). More importantly, the temperature dependence of the oxygen potential of such a fuel specimen suggests that it is governed by the Mo/MoO_2 equilibrium [8]. However, the out-of-pile demonstration that such an equilibrium can actually impose itself upon an oxide fuel remains to be established. Note that at 750°C, the niobium dioxide/pentoxide equilibrium, lies below the oxygen potential of a fresh UO_2 fuel at roughly -468 kJ/mol.

The first obstacle to overcome, before such additives can be used with the aim of reducing, cum eliminating, the risk of PCI induced SCC, is to produce a material with industrial grade characteristics, foremost of which is the microstructure. This has been the focus of a number of past studies [10, 6, 7]. The next step is to investigate if and under what conditions redox couples involving these additives actually form and/or whether they effectively impose their equilibrium oxygen pressure on the solid. It is this latter point we investigate

in this work.

To this end, the redox response of three different types of polycristalline materials have been investigated using the EMF (Electro-Motive Force) method. The three materials either contained molybdenum or niobium, or were free of additives. Experiments essentially involved subjecting these materials first to reducing conditions, and subsequently to conditions that are oxidising with respect to the redox equilibria liable to be activated. The oxygen activity of samples was monitored in situ using an electrochemical device and temperatures investigated ranged between 750 °C and 950 °C. A number of SEM examinations, along with EBSD or EDX analyses, were carried out prior to and following the high temperature experiments. One should note that the temperatures investigated are typical of fuel centreline temperatures under normal operating conditions in PWRs. Although this paper is relevant mainly in the context of PWR conditions, similar solutions aiming to act upon or control the oxygen activity of fuels in-pile could be developed for any type of oxide fuel. The redox couples just have to be chosen appropriately to suit the particular application and the effect one aims to mitigate.

The paper is organised as follows: section 2 is a description of how the materials we studied were manufactured. Section 3 provides details relative to the techniques applied in this work: microstructural characterisation methods and the experimental setup that was used to monitor *in situ* the response of materials to changing redox conditions. Section 4 is devoted to the microstructural characterisation of materials prior to the redox experiments. Experimental results are presented in section 5. These comprise both the *in situ* response of materials and the microstructural changes induced by the oxidizing conditions. In section 6, the results are discussed and concluding remarks are provided in section 7.

2. Materials manufacturing

All materials were manufactured from a dry route UO_2 powder using powder metallurgy processes. Following the incorporation of additives to the powder in appropriate conditions, green pellets were obtained by pressing at 450 MPa (see Table 1). The resulting samples were dense polycristalline, cylindrical pellets, roughly 8 mm in diameter. Twin samples that were not subjected to an electrochemical treatment were prepared with the aim to characterise the as-manufactured microstructure therefore providing a reference microstructure.

A word must be said about the choices made for sintering the Mo and Nb containing materials. The exact details of the manufacturing process in regard to the former additive may be found in reference [7]. In this case, sintering was performed in a two-stage tungsten capsule which was closed with a tightly fitting lid but not completely sealed. The bottom stage of the device was filled with an intimate mixture of metallic molybdenum and molybdenum dioxide, whereas green pellets were placed in the upper stage. The top and bottom stages were separated from each other by a perforated grid that facilitated equilibration of gas pressures in both compartments. It was surmised that sintering would

Sample type	Additives	Sintering conditions (hours)	Volume fraction of pores	Sample height
Reference UO_2 see [11]	none	1700 °C (4) Ar, 5%H_2	2 ±0.2 %	2.4 mm
Mo sample see [7] and text	0.5 wt.% Mo 1.5 wt.% MoO_2	1640 °C (4) Tungsten capsule	7 ± 1%	3.4 mm
Nb sample see [7]	1.6 wt.% NbO_2	1670 °C (4) Ar, 5%H_2	1.7 ±0.1% (open) 2.8 ±0.2% (closed)	3.6 mm

Table 1: Sample manufacturing and characteristics

occur in an oxygen partial pressure corresponding to the Mo/MoO_2 equilibrium, therefore preserving the two forms of the redox couple. The closed capsule was placed in the region of an alumina furnace of uniform temperature and heated in a flowing gas mixture of pure argon. This method was proved to produce a material with a reasonably high density. Applying the same method to the Nb containing material was found to produce a material with too low a density whereas, sintering under a reducing atmosphere, see Table 1, did not. In this latter case, an additional post-sintering, annealing step at 1400°C was applied at an appropriate oxygen potential, in order to convert all potentially reduced forms of niobium oxide, to niobium dioxide only. It was surmised that the activation of the NbO_2/Nb_2O_5 couple could be carried out *in situ*. The amount of niobium dioxide to add to uranium dioxide is estimated so that, in the event that buffering actually works in-pile, NbO_2 can absorb the entire quantity of O released by fission, up to a burnup of approximately 40 GWd/Mt.

3. Experimental techniques

3.1. Electrochemical principles and device

Possibly the most straightforward way of ascertaining the solid state oxygen activity of a non-stoichiometric sample, is to monitor the Nernst voltage, or EMF, or Open-Circuit Voltage (OCV), that appears across an electrochemical chain comprising a reference platinum electrode, a solid-state electrolyte (a 2 mm thick Yttria Stabilised Zirconia (YSZ) disk or membrane), the sample to be characterised, itself in intimate contact with a second platinum electrode. A schematic diagram of the setup is shown in Figure 1. A much more detailed account of the device we have developed may be found elsewhere [12]. We must now make a number of comments that are key to understanding our results. Firstly, under the assumption of thermodynamic equilibria at both electrodes,

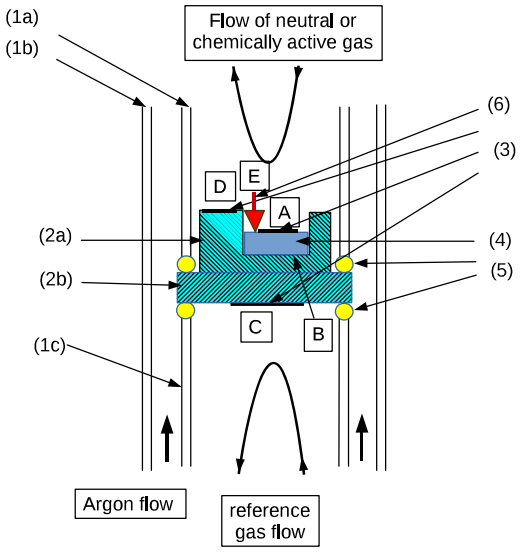

Figure 1: Schematic representation of the electrochemical device for characterising the solid state oxygen activity of a Mixed Ionic–Electronic Conductor (MIEC). A solid state electrolyte, in our case YSZ membrane, is exposed on one side to a reference gas of known activity, and is on its other side, in close contact with the non-stoichiometric sample to be characterised: (1a) upper alumina tube; (1b) outer alumina tube; (1c) lower alumina tube; (2a) YSZ. sample holder; (2b) YSZ. membrane; (3)platinum deposits; (4) MIEC sample; (5) gold O–rings. A, B, C and D refers to the points between which electrical potentials are measured (A, C, D) or enter into the analysis (B); (6) YSZ. cone shaped tip and platinum lead.

the OCV or EMF ($U_A - U_C$) of the cell is given by the following relationship:

$$U_A - U_C = \frac{\mathrm{R}T}{4.\mathscr{F}} \mathrm{Ln}(\frac{p^M_{O_2}}{p^A_{O_2}}) \quad (1)$$

In this expression, T is the homogeneous temperature of the device, R and $\mathscr{F}$ are the ideal gas and Faraday constants respectively and $p^C_{O_2}$ is the equilibrium oxygen partial pressure at the reference electrode. If the MIEC is homogeneous, $p^M_{O_2}$ is the uniform oxygen activity in the bulk solid. If the MIEC is inhomogeneous, we have shown [13] that in the case of an electronic conductor such as UO_{2+x}, $p^M_{O_2}$ is the oxygen activity in the sample, but at the interface with the solid state electrolyte. The device has a number of additional features:

- the sample may be exposed to either purified argon or a mixture of argon, hydrogen and water vapour which enables a buffered reaction to be set up in the gas phase.
- YSZ electrochemical oxygen gauges are placed at the gas inlet and outlet of both the reference and sample compartments of the device and maintained at constant temperatures between 650 °C and 680 °C.
- a platinum contact placed on the YSZ membrane provides an *in situ* measurement of the oxygen partial pressure of the gas phase adjacent to the sample: $U_D - U_C$ in Figure 1.
- a YSZ point electrode can be placed in contact with the surface of the sample (see [14]). Although this measure was not used systematically, it can provide very useful information relating to the oxygen activity of the sample surface. So, the EMF of the cell provides the oxygen activity at the YSZ membrane sample interface and the YSZ point electrode the oxygen activity of the solid at the upper surface.
- the reference oxygen partial pressure ($p^C_{O_2}$ in relationship 1) is controlled and measured using an oxygen pump and gauge system and a flowing gas mixture of argon. Di-oxygen is incorporated to the gas flow using the YSZ electrochemical pump. The reference oxygen pressure is monitored continuously and remained stable throughout the experiments at a value of roughly 100 ppm. This helps limit the potentially deleterious effect of oxygen permeation through the YSZ electrolyte of Figure 1 [14] .

3.2. Microstructural characterisation

Four, either molybdenum or niobium containing pellets were prepared with the aim to characterise their microstructure prior to and following the electrochemical treatment. The two control samples, *i.e.* those which were not subjected to an electrochemical treatment were observed across a polished circular section of the pellet. Following the electrochemical experiment, the two niobium and molybdenum doped samples were cut through a plane containing the axis of symmetry, so as to reveal potential differences in the microstructure

between regions located at the surface directly exposed to the carrier gas, in the bulk, and at the interface between the YSZ and the specimen. Because they were exceedingly brittle following the treatment, the molybdenum and niobium doped samples were mounted in resin. Samples were polished for SEM observation using decreasing grain sizes and the final step in this preparation process involved the use of a colloidal silica suspension.

SEM examinations were performed using a FEI Nova NanoSEM 450 microscope, equipped with a 150 mm^2 silicon drift detector for EDX and a symmetry EBSD detector from Oxford Instruments, both operated using the AZTEC software. EBSD data were processed using the AZTEC Crystal software.

4. Microstructural characterisation of materials in the as-manufactured state

4.1. Fuel material containing Mo as an additive

Figure 2a is a Back-Scattered Electron (BSE) image of a 420×290 μm^2 area which reveals a phase contrast: the uranium dioxide matrix corresponds to the brighter regions. Variations in grey levels between grains are due to differences in crystallographic orientations. Pores left over from the manufacturing process and secondary phases appear as darker regions both within the grains and at the grain boundaries. Figure 2b is an X-ray distribution map of molybdenum acquired using EDX over an area identical to that of Figure 2a. It shows that the intermediate grey-level regions in the BSE image (Figure 2a), are rich in molybdenum, and that probably two phases of differing Mo-concentration are present. To ascertain this latter point, EBSD analyses were performed over the same area. Figure 2c is the resulting phase map.

The different colours correspond to the phases that are indexed: bcc molybdenum in blue, monoclinic MoO_2 in yellow and fluorite UO_2 in red. A high proportion (roughly 98 %) of the analysed surface is indexed with a high confidence level. Pores or polishing defects (in recess with respect to the plane of observation) cannot be indexed. Figure 2c shows that aggregates contain either one or the other or both redox forms of molybdenum. Further evidence of the presence of two redox forms of molybdenum (metal and oxide) in the as-sintered pellet may be found in Section 1 of the suplementary material section. SEM/EBSD characterisations of a section of the pellet, reveals some degree of inhomogeneity (presence of cracks, size distribution of molybdenum rich aggregates, grain size...). Three regions (roughly 840 × 580 μm^2), two located towards the centre of the pellet and one at the pellet periphery were characterised using EBSD. The Equivalent Circle Diameter (ECD) of grains was estimated at 10.5 and 14.5 μm for the regions located in the pellet centre and 18.5 μm for the peripheral region.

4.2. Fuel material containing Nb as additive

SEM/EDX and EBSD characterisations revealed:

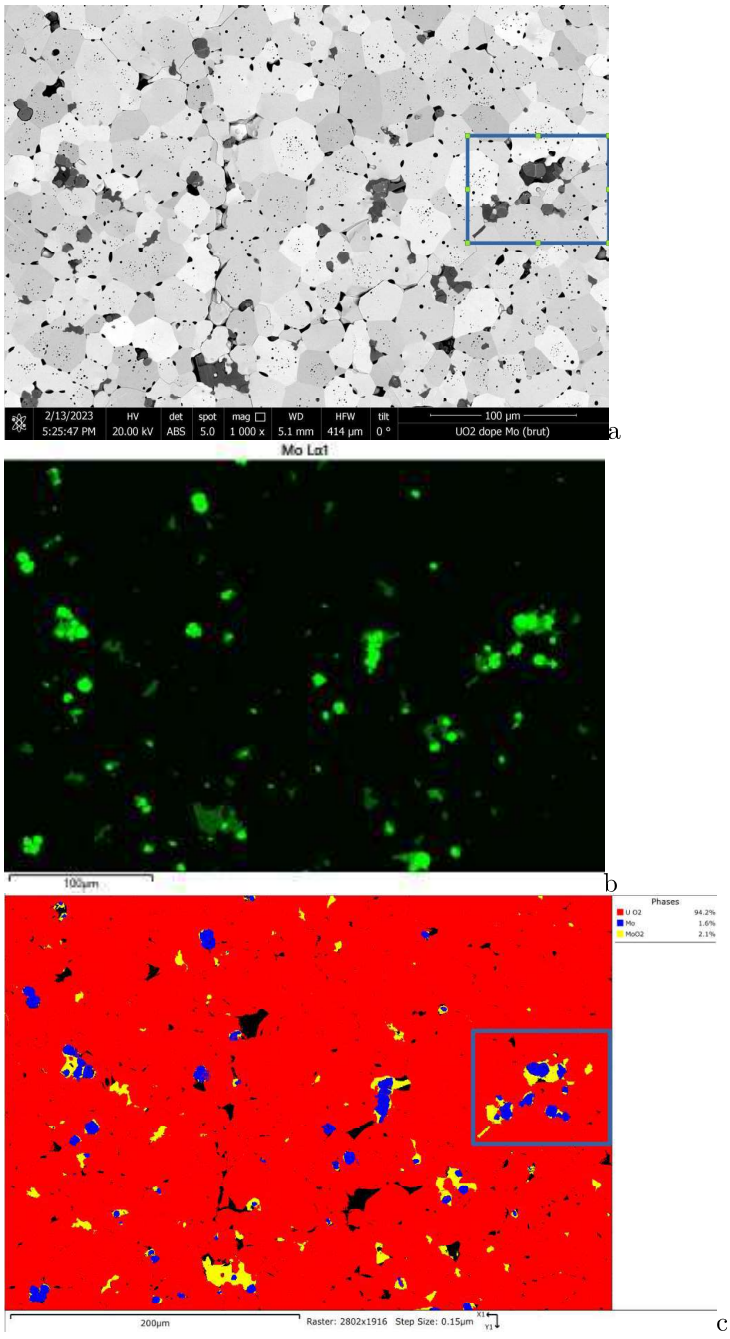

Figure 2: Microstructural characterisation of an as-sintered, Mo-doped pellet: (a) BSE image revealing a phase contrast; (b) Mo X-ray map obtained from an EDX analysis; (c) EBSD phase analysis with different phases indexed as bcc Mo (blue), monoclinic MoO_2 (yellow) and fluorite UO_2 (red); Regions that cannot be indexed in (c) are shown to lie below the observation plane, *i.e.* manufacturing pores, cracks or regions with imperfections left over from polishing.

- the presence of a unique niobium phase in a dioxide form. EDX analyses of niobium rich aggregates enabled the O/Nb ratio to be estimated at 2.01 $\pm$ 0.02 from 10 measurement points. EBSD data showed the presence of NbO_2 in a tetragonal form exclusively [15]. Note that NbO_2 has a rutile structure at high temperature but undergoes a phase transition at 810 °C. In the low temperature tetragonal phase, it is reported that the structure is only slightly distorted from rutile [16].

- An average ECD was estimated at 24 μm, from the analysis of two central areas of the pellet each comprising approximately 650 grains.

5. Results

Having increased the samples' temperature under reducing conditions, a constant composition $Ar/H_2/H_2O$ gas mixture was then set up in the gas phase, such that the oxygen potential of the gas lay above both the NbO_2/Nb_2O_5 and Mo/MoO_2 equilibria at all temperatures. The actual experiments then involved subjecting the samples to very similar temperature changes whilst simultaneously monitoring their EMF. A change in temperature displaces the gas phase equilibrium and therefore modifies the thermodynamic conditions the samples are exposed to. Details relating to experimental conditions may be found in Section 2 of the supplementary material section.

5.1. EMF response of samples to oxidizing conditions

Changes in sample oxygen partial pressures derived from the OCV for all three samples are shown as a function of time in Figures 3a, 3b, and 3c, relative to the molybdenum doped, niobium doped and the additive free UO_2 samples respectively. Indicated in these figures are the samples' temperature changes and the *in situ*-measured oxygen activity of the gas phase during all three experimental sequences. Also shown in these figures are the expected equilibrium oxygen partial pressures relative to the Mo/MoO_2 equilibrium (Figure 3a) and to the NbO_2/Nb_2O_5 equilibrium (Figure 3b). Equilibrium partial pressures were derived from JANAF tables [9].

There are three outstanding features that transpire from Figures 3a, 3b and 3c:

- changes in the solid-state oxygen activity of samples containing additives follow with changes in temperature.

- the oxygen activity of the solids containing additives remains intermediate between that of the gas phase and the Mo/MoO_2 or NbO_2/Nb_2O_5 equilibria.

- by contrast, although the oxygen activity of the solid containing no additives (Figure 3c) follows, in the main, changes in the sample temperature, its actual value lies above that of the gas phase, indicating the material is out of equilibrium.

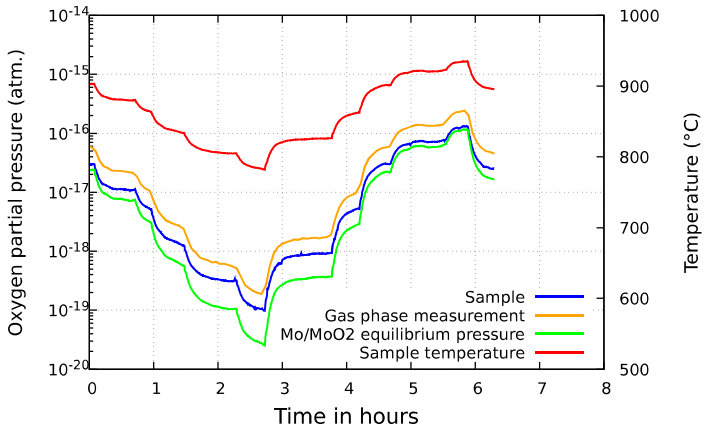

(a)

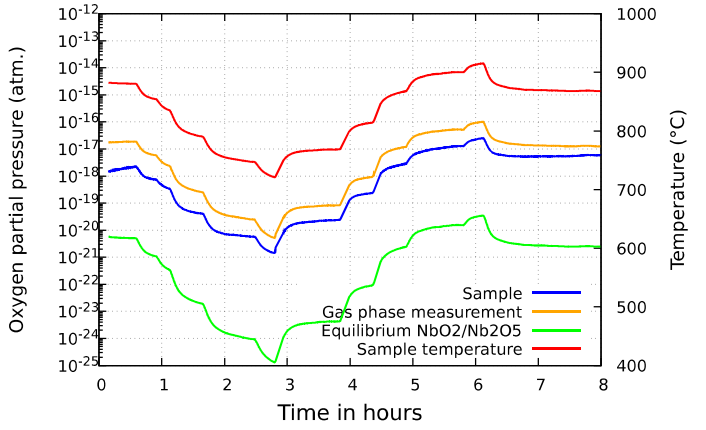

(b)

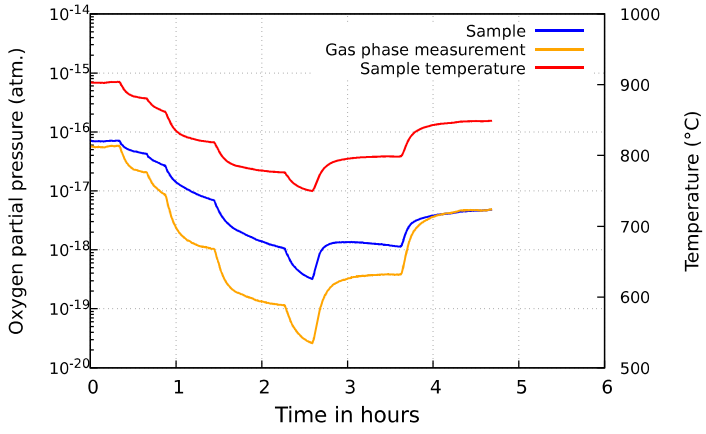

(c)

Figure 3: Changes in oxygen activity in the gas phase and the three samples as a result of temperature cycling. (a) sample containing molybdenum; (b) sample containing niobium; (c) sample containing no additives. Also indicated are the equilibrium oxygen partial pressures for the Mo/MoO_2 (a) or NbO_2/Nb_2O_5 (b) redox couples.

5.2. Post-experiment microstructural characterisation of materials

Following the redox treatment in the electrochemical cell, both the molybdenum and niobium containing samples were cut through a plane containing a diameter and the resulting sections were polished and observed. Manipulation of the specimens revealed they were particularly brittle, to the extent that a fragment from the niobium oxide containing sample located at its surface, detached itself from the bulk specimen.

5.2.1. Molybdenum-containing sample

The sample brittleness was confirmed by SEM examinations. Figures 4a, b and c are BSE images (roughly 820 × 540 μm^2) of the sample taken from different positions, in close proximity to the surface directly exposed to the carrier gas (Figure 4a), at an intermediate position (Figure 4b), and close to the interface between the sample and YSZ membrane (Figure 4c).

The sample shows a decreasing level of cracking as one moves away from the surface exposed to the carrier gas. In Figure 4a in particular, the cracks, which are essentially intergranular in nature, appear to interconnect molybdenum rich particles at the grain boundaries.

5.2.2. Niobium-containing sample

SEM images of a section of the sample also reveal an extensive network of intergranular cracks that appear to interconnect niobium rich particles. Figures 5a and b are BSE images on a similar scale of two regions of samples containing additives, prior to and following our electrochemical treatment. A number of points may be made in relation to these microstructures:

- in both of the samples, aggregates are clearly visible as they take on a uniform, intermediate shade of grey, between the bright UO_2 matrix background and the darker pore structure or crack network, indicating the presence of a lower density phase.
- An average of about ten EDX analyses of intermediate grey areas similar to those seen in Figure 5b indicate an oxygen to niobium ratio of 2.49 ± 0.07, so close to the ratio for niobium pentoxide.

In order to confirm the extent to which niobium dioxide has been converted to niobium pentoxide as a result of the electrochemical characterisation, and to ascertain the nature of the phases present, EBSD analyses were carried out on samples before to and after the electrochemical treatment. Figures 6a and 6b are large area phase maps derived from those analyses. In both cases, the phases we sought to index were, fluorite UO_2, tetragonal NbO_2 [15], and monoclinic Nb_2O_5 [17, 18, 19]. The monoclinic form was chosen from possible alternatives since it is reported to be the high temperature form of the pentoxide (H-Nb2O5) [20, 18]. A small fraction of the surface cannot be indexed due to surface imperfections such as pores, or resulting from the fact that some grains may have been torn away during sample preparation. In Figure 6a, tetragonal NbO_2 is practically

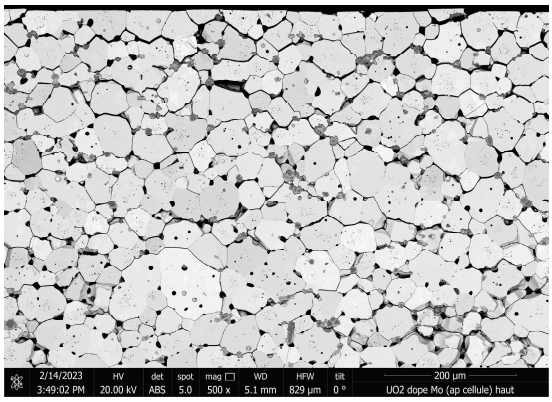

(a)

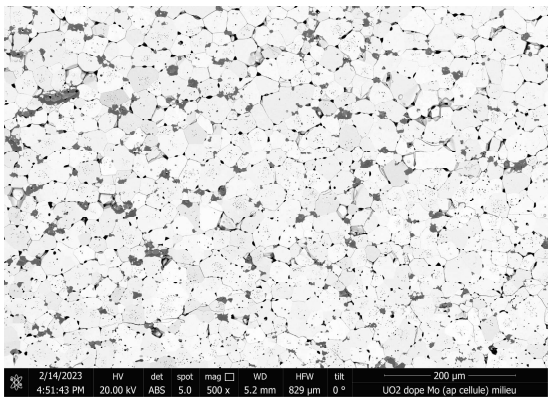

(b)

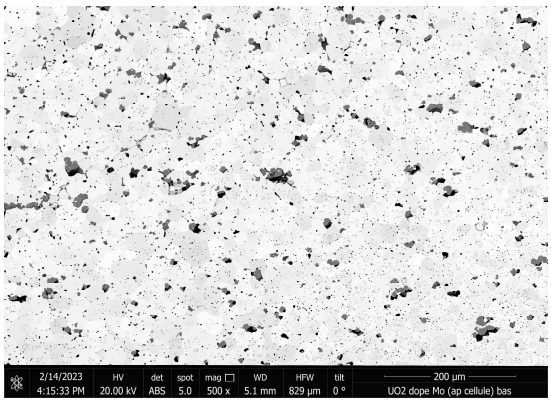

(c)

Figure 4: BSE images roughly $820 \times 540\ \mu m^2$ of the molybdenum containing sample following its electrochemical characterisation, (a) close to surface exposed to the oxidising carrier gas, (b) at an intermediate position in sample and (c) close to the interface with the YSZ membrane. The phase-contrast of BSE images reveals the molybdenum rich samples as having a darker shade of grey than the background UO_2 matrix. The region exposed to gas (Figure (a)) shows a network of intergranular cracks that interconnect the molybdenum rich particles. In addition, most of these molybdenum rich particles systematically bear two shades of grey, characteristic of the two forms of the Mo redox couple (Mo and MoO_2).

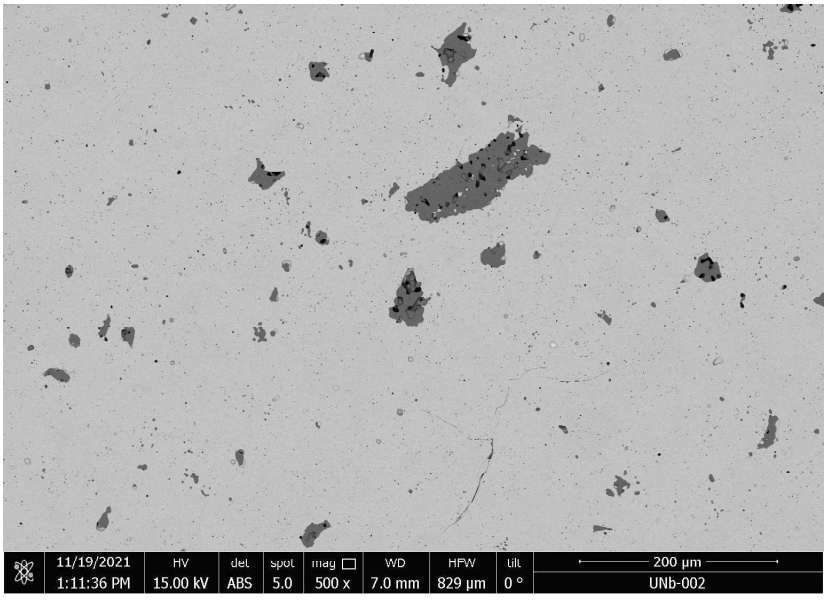

Figure 5: BSE images of areas of the Nb doped pellets, roughly 830 × 550 μm^2 and 1040 × 690 μm^2 respectively prior to (a) and following (b) electrochemical treatment. Niobium oxide agglomerates appear as areas in which the shades of grey are intermediate between the bright background (denser UO_2 matrix) and the dark pore structure or crack network.

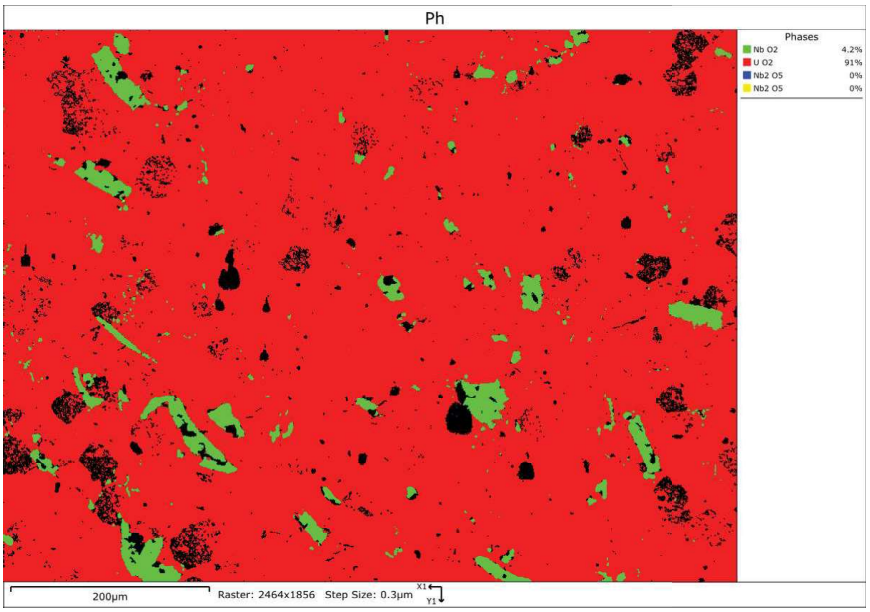

Figure 6: Phase maps obtained from EBSD prior to (a) and following (b) the redox treatment. Prior to it, niobium aggregates comprise essentially tetragonal niobium dioxide (in green), whereas following it, they are largely made up of a monoclinic form of niobium pentoxide (in blue).

the only niobium form. Following the electrochemical treatment, this phase has transformed to monoclinic niobium pentoxide.We have checked by running similar EBSD analyses, that, in the regions the least exposed to the carrier gas, *i.e.* towards the interface between the sample and the YSZ membrane, the proportion of niobium dioxide remains low (less than 10% of the total surface of niobium oxide phase). In this case, the dioxide appears in the form of inclusions contained within larger niobium pentoxide aggregates.

Finally, because it has been reported in the literature that complex ternary U-Nb-O phases may exist [21, 22, 23] and in addition, that the redox couple NbO_2/UNb_2O_7 may be activated in samples of similar composition to ours [7], we studied several niobium pentoxide aggregates at greater magnification, using BSE and SE imaging. We focussed especially upon the interface between the particle and the matrix. Such observations are reported in Figures 7a, 7b. Figure 7a shows a niobium pentoxide particle, characterised by an intermediate shade of grey, embedded in a UO_2 matrix at the intersection of several grains. The image shows that there exists a thin layer of thickness of the order of a micron surrounding the particle. This thin layer's grey level, which is intermediate between that of the UO_2 matrix and that of the niobium pentoxide particle, could suggest the presence of a new phase of intermediate density. However, it is too thin to allow for an accurate EDX analysis due to contributions of its surroundings. Figure 7b, which is a secondary electron image and is sensitive to topography, reveals that the particle as a whole, is in recess. The thin layer is in fact at an intermediate altitude between the pentoxide particle itself and the matrix. The "phase contrast" seen in 7a is therefore probably not characteristic of a new phase. This feature was observed for all the particles we studied but one would have to characterise this particle-matrix interface using a more spatially resolved method, such as transmission electron microscopy, in order to draw definitive conclusions.

6. Discussion

Our observations, whether they concern EMF monitoring at the macroscale, or whether they involve SEM analyses of the microstructure, all purport to indicate substantial electrochemical activity strongly influenced by the presence of niobium oxides or molybdenum in several redox forms. In the following we discuss these results in the light of various material properties. We first focus on EMF measurements and subsequently upon microstructural changes, which the various materials have undergone.

6.1. EMF measurements

The electrochemical response of the two doped samples to changes in the oxygen activity of the gas phase are qualitatively similar. Firstly, the oxygen activity at the sample-electrolyte interface establishes itself at an intermediate value between that prescribed by the redox couples (green lines in Figures 3a and 3b determined by the $Mo + O_2 \rightleftarrows MoO_2$ or $2NbO_2 + \frac{1}{2}O_2 \rightleftarrows Nb_2O_5$

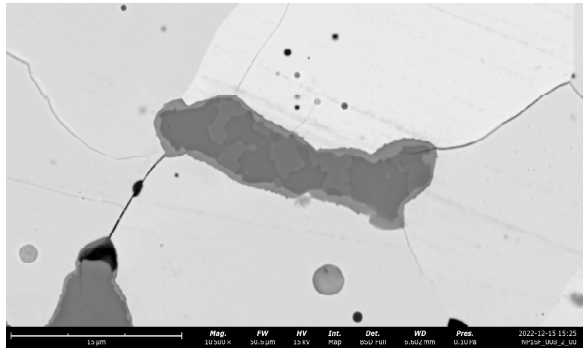

(a)

(b)

Figure 7: Analysis of a niobium rich particle in the niobium-doped UO_2 sample following the electrochemical treatment (a) BSE image of an area comprising a niobium pentoxide particle embedded in the UO 2 matrix. The particle has a shade of grey which is intermediate between the lighter coloured matrix and darker pores or open grain boundaries; (b) SE image which shows that the niobium pentoxide particles are in recess as a result of the surface preparation process. The thin layer that appears to surround the particle in the BSE image stands out probably because it is at an altitude intermediate between the bulk particle and the UO_2 matrix. It is also possible that a ternary U-Nb-O phase has formed but a better resolved technique is warranted to conclude

.

equilibria) and that imposed by the sweep gas (*i.e.*, the $H_2 + \frac{1}{2}O_2 \rightleftarrows H_2O_{vap.}$ equilibrium). Secondly, in both cases, the kinetics of these changes are fast and closely correlate to the change in temperature. This is not the case for the undoped sample, the OCV or oxygen pressure of which is governed by substantially slower kinetics. The contrast between the response of the uranium dioxide sample containing no additives and the doped samples suggests a strong influence of the additives.

Let us assume that the oxygen gas-solid exchange is essentially controlled by first order reaction rates and let us further assume that these reactions are the rate controlling mechanisms. In this case, the average oxygen concentration in the sample C_O may be describe by the follwoing first order differential equation:

$$\frac{dC_O}{dt} = k_{gs}(C_g - C_O) + k_{ss}(C_{eq.} - C_O) \tag{2}$$

where C_g is the oxygen concentration in the gas phase (*i.e.* the oxygen concentration in a UO_2 solid of identical oxygen activity to that of the gas phase), $C_{eq.}$ is the oxygen concentration in a UO_2 solid determined by the presence of both redox forms of the additives. This concentration corresponds therefore either to the NbO_2/Nb_2O_5 or the Mo/MoO_2 equilibria; k_{gs} is the UO_2/gas oxygen exchange coefficient and k_{ss} the oxygen exchange coefficient between the colocalised forms of the redox additives and the UO_2 matrix.

Solving equation (2) assuming $C_{eq.}$ et C_g are constant, provides the average oxygen concentration in the sample which approaches the following steady-state value:

$$C_O(\infty) = \frac{k_{gs} \times C_g + k_{ss} \times C_{eq.}}{k_{gs} + k_{ss}} = (1 - \alpha) \times C_g + \alpha C_{eq.} \tag{3}$$

where $\alpha = \frac{k_{ss}}{k_{gs}+k_{ss}}$. α is a real number between 0 and 1 depending on the rate limiting exchange mechanism (*i.e.* gas - solid or solid-solid). The value of $C_O(\infty)$ is limited by its higher and lower bounds, C_g and $C_{eq.}$, which is consistent with the fact that in Figures 3a and 3b, the sample oxygen partial pressure remains bounded by that of the gas and the supposed redox equilibria. This is typical of non-stoichiometric oxide systems exposed to two competing redox equilibria.

Figure 3a specifically reveals that as the temperature of the molybdenum doped sample approaches 900°C, its oxygen activity approaches the value of the Mo-MoO_2 equilibrium, suggesting that temperature is conducive to improved particle-matrix oxygen exchange. The observation that stands out in Figure 3b is that as the temperature is maintained towards the end of the experiment, the buffering effect in the niobium doped sample appears to wear off, by contrast with the molybdenum doped sample. Indeed, as a result of the initial niobium and molybdenum additions (see section 2), the total buffering capacity of the molybdenum doped material (defined as the total number of oxygen atoms which may be consumed by the additive contained in one gram of uranium dioxide) is roughly five times greater than that of the niobium doped sample.

6.2. Microstructural observations

The most obvious microstructural sign of a strong redox activity is the extent to which fuel cracking has occurred in the samples containing additives (see 5.2). Material fragmentation with intergranular cracks forming a network linking up aggregates between them, is a sure sign of changes in the volume of these aggregates as they oxidise or reduce depending on the surrounding redox environment. Molybdenum crystallises in a bcc structure which has a density of 10.22 g/cm^3 whereas the monoclinic form of molybdenum dioxide which the EBSD analysis reveals has a density of 6.47 g/cm^3 [24]. Niobium dioxide at room temperature is described as a superstructure with a subcell of the rutile type and a density of 5.92 g/cm^3 [15] and niobium pentoxide is reported as having a density of 4.55 g/cm^3 [17]. In the current set of experiments, temperatures did not exceed 950°C, hence the UO_2 matrix remains brittle and such particle volume changes will likely induce local stresses sufficient for the material to fracture.

Fuel cracking, should it occur to this extent in reactor, is obviously likely to lead to undesirable fission product release. However there are substantial differences in the conditions in which our experiments are carried out and the expected situation in-pile. In-pile, if oxidation of the additives is kinetically possible, the release of oxygen from fission events, hence its absorption by particles, will occur very slowly, over periods of the order of years rather than minutes or hours, thus enabling the material to accommodate mechanical strains induced by these volume changes. An indication that the kinetics with which oxygen is made available influences the extent to which the matrix breaks up may be seen from the fact that cracking is concentrated in the regions directly exposed to the carrier gas. In the molybdenum doped sample in particular (see Figure 4), the region of the sample farthest away from the surface shows hardly any sign of cracking, by contrast with the region closest to it. Also, under irradiation, radiation induced deformations will enable the UO_2 matrix to better accommodate expected strains resulting from particle swelling.

EBSD results relating to the niobium doped sample leave no doubt as to the quasi-complete oxidation of the originally reduced form of the niobium oxide and is entirely consistent with the fact that the buffering effect was wearing off towards the end of the experiment. We have also mentioned the fact that, after this effect had worn off for the first time (prior to the data collection reported in Figure 3b), we were able to reactivate the buffering effect by exposing the sample to reducing conditions. This illustrates the reversibility of the phenomenon and the versatility of the doping agent. Regarding the molybdenum sample, we also carried out five complementary EBSD analyses over large areas (roughly 840×560 μm^2) and at different positions between the surface and YSZ-sample interface following our experiments. These showed clear signs of changes in the proportion of the oxide to metal molybdenum phases: one area was located at the YSZ-sample interface; two were located in the bulk of the sample, roughly equidistant from the upper and lower surfaces of the sample; one was located in a region directly exposed to the carrier gas. The four former regions showed a high proportion of molybdenum in an oxide form (between 80 and 90 %), consistent

with the overall oxidation of the sample during the experiment. Only the region located in close proximity to the area exposed to the carrier gas contained a high proportion of molybdenum in a metal form. This is no doubt due to the fact that towards the end of the experiment, the oxygen partial pressure of the carrier gas used was well below that of the Mo/MoO_2 equilibrium, presumably inducing limited reduction of the molybdenum dioxide phase. In comparison, similar EBSD analyses of the sample prior to the experiment revealed a proportion of the oxide phase in the region of 60 %.

6.3. Possible in-pile behaviour

We have mentioned some caveats in using the results of the experiments reported here to predict the behaviour of these fuels in-pile. In this context, an issue to tackle is whether a fuel containing an additive in its reduced form only, would actually have the desired property of buffering the oxygen partial pressure under irradiation. Under Fast Breeder Reactor conditions, direct EMF measurements have definitely shown fission to be an oxidising process [25]. This is less clear from results of EMF characterisations of fuels irradiated under Pressurised Water Reactor conditions, but should be the case from our knowledge of fission yields and valence states of fission products [26]. EMF measurements up to high burnups indicate that the oxygen potential of the material remains close to that of the Mo/MoO_2 equilibrium [8] as oxygen released by fission is consumed through partial oxidation of the zircaloy cladding and progressive oxidation of metallic molybdenum [8]. The fact that the NbO_2/Nb_2O_5 equilibrium oxygen partial pressure is extremely low (corresponding to deviations from stoichiometry below 10^{-3} at 900°C for UO_2) means that as oxygen is released from fission in the early stages of the irradiation process, the redox couple should immediately activate and maintain the oxygen partial pressure corresponding to this equilibrium throughout the fuel lifetime. But clearly, in-pile testing is required for this to be proved for certain.

7. Conclusions

We have demonstrated that it is possible to buffer the oxygen activity of a uranium dioxide fuel in a 750-950 °C temperature range, by incorporating molybdenium or niobium in separate phases.

The demonstration is based on an EMF study of three uranium dioxide samples: one that contains both metallic molybdenum and molybdenum dioxide, one that contains niobium dioxide only, and the last that contains no additives other than impurities left over from the manufacturing process. The samples are exposed to an oxidising, chemically active, flowing gas mixture, whose oxygen partial pressure lies above the partial pressures required to oxidise molybdenum. Their electrochemical response is such that their oxygen activity lies between that of the gas mixture and the oxygen pressure of either the Mo/MoO_2 or NbO_2/Nb_2O_5 equilibria. The response of the UO_2 sample containing no additives is radically different.

The conclusions are compounded by a SEM study comprising SE and BSE imaging, EDX and EBSD analyses, which shows that the doped samples are prone to cracking as a result of volume changes of the dopant containing aggregates. As regards the molybdenum doped material, the fraction of molybdenum dioxide following the oxidising treatment increases substantially. We also show that practically all the niobium dioxide has been converted to niobium pentoxide. Both these observations are consistent with the redox changes imposed upon the samples. In particular, towards the end of the EMF study, the niobium doped material loses its ability to buffer the oxygen activity of the sample.

Of course these conclusions are not entirely surprising when one considers thermodynamic equilibria. The point here though is that, at those temperatures, there are no kinetic limitations to the transfer of oxygen between the UO_2 matrix and the different redox aggregates. Furthermore, in the case of niobium, we show that buffering is reversible in the sense that if aggregates are entirely oxidised, they can revert to a reduced form if the thermodynamic conditions are favourable, thus reactivating the buffering effect. No p̂hase other than niobium dioxide or pentoxide is observed, despite reports in the literature of stable U-Nb-O ternary phases.

The level of cracking observed in our experiment is not satisfactory for a nuclear fuel as it would probably lead to unacceptable levels of fission product release in pile. There are reasons to believe though, that in reactor, the redox changes imposed would occur over much longer periods of time thus enabling the material to accommodate local strains induced by aggregate swelling. The next step in this study is therefore to carry out in-reactor experiments in order to ascertain the ability of such materials to control the oxygen partial pressure of fuels under irradiation.

References

[1] V. Peres, *Contribution à l'étude de la dispersion de particules secondaires dans le dioxyde d'urnaium polycristallin*, Ph.D. thesis, Institut National Polytechnique de Grenoble (1994).

[2] L. Bourgeois, *Contribution à l'étude du rôle de dopants dans la densification et la croissance cristalline du dioxyde d'uranium*, Ph.D. thesis, Université de Grenoble (1992).

[3] J. C. Killeen, J. Nucl. Mater. **88**, 185 (1980).

[4] P. Konarski, J. Sercombe, C. Riglet-Martial, L. Noirot, I. Zacharie-Aubrun, K. Hanifi, M. Frégonèse, and P. Chantrenne, J. Nucl. Mater. **519**, 104 (2019).

[5] C. Riglet-Martial, M. Brothier, P. Matheron, V. Pennisi, and V. Basini, Combustible nucléaire régulateur des produits de fission corrosifs additivé par au moins un système oxydo-réducteur (2013), eP 2 917 917 B1.

[6] V. Pennisi, *Contribution to the identification and the evaluation of a doped UO2 fuel with controlled oxygen potential*, Theses, Université de Bordeaux (2015).

[7] M. Khair, *Oxydo–réduction et spéciation des produits de fission corrosifs dans les combustibles oxydes. Évaluation des bénéfices d'un combustible tamponné en* p_{O2}, Thèses, Université de Bordeaux (2019).

[8] H. Matzke, J. Nucl. Mater. **208**, 18 (1994).

[9] M. W.Chase, *NIST-JANF Thermochemical tables* (J. Phys. Chem. Ref. Data, 1998).

[10] J. Killeen, Tech. Rep. RD/B/N3374 (Central Electricity Generating Board, Berkeley Nuclear Laboratories, UK, 1976).

[11] M. Salvo, *Étude expérimentale et modélisation du comportement mécanique du combustible* UO_2 *en compression à haute température et forte vitesse de sollicitation*, Ph.D. thesis, Aix–Marseille Université (2014).

[12] P. Garcia, M. C. Steil, A. Miard, E. Douguet-Bronnec, F. Fourne-Fayard, and J. Fouletier, Solid State Ionics **370**, 115705 (2021).

[13] P. Garcia, Relationship between crystal defects and engineering properties in non-stoichiometric oxides with a focus on nuclear oxide fuels, Thèse d'Habilitation à Diriger des Recherche, Aix–Marseille Université (2022).

[14] M. Steil, J. Fouletier, and P.-M. Geffroy, J. Membr. Sci. **541**, 457 (2017).

[15] A. K. Cheetham and C. N. R. Rao, Acta Cryst. B **32**, 1579 (1976), https://onlinelibrary.wiley.com/doi/pdf/10.1107/S0567740876005876 .

[16] R. Pynn, J. D. Axe, and R. Thomas, Phys. Rev. B **13**, 2965 (1976).

[17] B. M. Gatehouse and A. D. Wadsley, Acta Cryst. **17**, 1545 (1964).

[18] E. Ko and J. Weissman, Catal. Today **8**, 27 (1990), catalytic conversion with niobium materials, Proceedings of the Niobium and Catalysts Symposium at the 1989 International Chemical Congress of Pacific Basin Societies.

[19] E. S. Crawford and J. S. Anderson, Philos. Trans. R. Soc. A **304**, 327 (1982), https://royalsocietypublishing.org/doi/pdf/10.1098/rsta.1982.0015 .

[20] K. Kato, Acta Cryst. B **32**, 764 (1976), https://onlinelibrary.wiley.com/doi/pdf/10.1107/S0567740876003944 .

[21] P. Mirwald, *Untersuchungen kristalliner mischphasen im system U-Nb-O*, Theses, Ludwig–Maximilians–Universität, München (1971).

[22] P. Mirwald and H. Schrocke, N. Jb. Miner. Abh. **125**, 201 (1975).

[23] C. Miyake, S. Ohana, S. Imoto, and K. Taniguchi, Inorg. Chim. Acta **140**, 133 (1987).

[24] B. G. Brandt and A. C. Skapski, Acta Chem. Scand. **21**, 661 (1967).

[25] H. Matzke, J. Ottaviani, D. Pellottiero, and J. Rouault, J. Nucl. Mater. **160**, 142 (1988).

[26] P. Garcia, J. Piron, and D. Baron (Nuclear Fuel Cycle and Materials Section, IAEA-TECDOC-957, 1994) pp. 523–538, proc. Symp. On Water Reactor Fuel Element Modelling at High Burnup and its Experimental Support, Winderemere, UK.

dateDecember 19, 2024

Contents